Microsphere-assisted super-resolution optical imaging of oriented silver nanowire arrays with polarized light

Farid Mahfoud, Christophe Cordier, Sebastien Marbach, Michel Tschopp, Paul Montgomery, Olivier Felix, Matthias Pauly, Manuel Flury

Optics & Laser Technology 191 (2025) 113383

Contents lists available at ScienceDirect

Optics and Laser Technology

journal homepage: www.elsevier.com/locate/optlastec

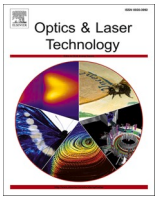

Full length article

Microsphere-assisted super-resolution optical imaging of oriented silver nanowire arrays with polarized light

Farid Mahfoud [a,b,*], Christophe Cordier [a], Sebastien Marbach [a], Michel Tschopp [b], Paul Montgomery [a], Olivier Felix [b,*], Matthias Pauly [b,c,*], Manuel Flury [a,*]

[a] ICube, Université de Strasbourg, CNRS, INSA, F-67000 Strasbourg, France
[b] Université de Strasbourg, CNRS, Institut Charles Sadron UPR-22, F-67200 Strasbourg, France
[c] ENS de Lyon, CNRS, LCH, UMR 5182, F-69342 Lyon, France

A B S T R A C T

Microsphere-assisted microscopy is a label-free imaging technique capable of surpassing the diffraction limit of conventional optical microscopes. This study investigates the imaging of oriented silver nanowire (AgNW) monolayers as a function of incident light polarization using a 30 μm diameter microsphere. Two types of AgNW arrays, fabricated by a "bottom-up" technique and e-beam lithography, are analyzed. Using a home-built optical microscope, the relationship between microsphere magnification and image contrast is explored to identify the optimal position for maximum contrast. The developed optical setup demonstrates at least a twofold resolution enhancement and permits to effectively visualize the optical anisotropy of nanostructured samples by tuning the polarization of incident light. These findings highlight the potential for further improvements in microsphere-assisted microscopy to achieve superior nanoscale resolution.

Topics: Microsphere-assisted microscopy, oriented silver nanowires, polarization, resolution enhancement.

1. Introduction

As technology progresses towards miniaturization, the necessity for the resolution of smaller objects using conventional optical microscopes increases. However, their lateral resolution limit of approximately $\lambda/2$ at best due to diffraction [1], restricts the capacity to characterize nanostructured samples [2].

Many optical microscopy techniques, collectively termed as "super-resolved microscopy" or "nanoscopy" have been developed to overcome the diffraction barrier [3,4], such as Fluorescence PhotoActivated Localization Microscopy (FPALM) [5], Stochastic Optical Reconstruction Microscopy (STORM) [6], and Stimulated Emission Depletion Microscopy (STED) [7]. While very successful for many types of samples, they require specific sample preparation [7] and the use of fluorophores can be a big disadvantage since they can lead to photobleaching, phototoxicity, and cell death [8]. Label-free nanoscopic techniques, including microsphere-assisted microscopy (MAM) [9], are promising alternatives.

MAM has attracted considerable attention over the past decade following its introduction in 2011 by depositing a glass microsphere (MS) on a sample surface in front of the objective to achieve a claimed lateral resolution of up to 50 nm [9]. Other studies have confirmed that a lateral resolution of $\lambda/4 - \lambda/5$ can be attained [10,11].

Since 2011, there has also been considerable debate regarding the origin of this resolution enhancement and the corresponding properties. Initially, the theory of the photonic nanojet was proposed, but has since been demonstrated to be insufficient for explaining the resolution beyond $\lambda/3$ [10–13]. Alternative theories, including the occurrence of whispering gallery modes and the conversion of the evanescent wave into a propagating wave, have also been proposed [12–14]. However, these have been unable to fully elucidate the underlying principles governing MAM.

In addition, the contrast [15,16], the magnification [17], and other properties of the virtual image obtained by the microsphere have also been studied. While the size of the microsphere can be between 1–100 μm, the correlation between the field of view and resolution enhancement is inverse, with smaller microsphere sizes resulting in improved lateral resolution at the cost of a reduced field of view [17–19].

Although the origin of the resolution enhancement in MAM is not yet fully understood, the technique has nonetheless been widely applied in various domains, including nano-imaging [20,21], live-cell imaging [22], polarimetric microscopy [23], semiconductor metrology [24], and interferometric measurements [25].

In general, MAM utilizes a microsphere placed over the specimen,

* Corresponding authors.
E-mail addresses: farid.mahfoud@etu.unistra.fr (F. Mahfoud), olivier.felix@ics-cnrs.unistra.fr (O. Felix), matthias.pauly@ens-lyon.fr (M. Pauly), mflury@unistra.fr (M. Flury).

https://doi.org/10.1016/j.optlastec.2025.113383
Received 26 February 2025; Received in revised form 2 June 2025; Accepted 11 June 2025
Available online 17 June 2025

which increases the effective numerical aperture (NA) of the system. This enhancement allows for the collection of light at larger diffracted angles, improving the resolution compared to a system without the microsphere [26]. Over the past year, several articles have been published with the aim of fully understanding the physics behind the resolution enhancement of microspheres. In their review studying all the models and theories behind the super-resolution attained by using microspheres, V. Abbasian *et al.* suggested that the resolution enhancement is a local enhancement of the effective numerical aperture of the system, and that it is independent of the concurrency of the whispering gallery mode and the NA of the objective [26]. On the other hand, Maslov *et al.* claim that the generation of super-resolved images depends on coherent phenomena, such as the scattering of light into waves that "circulate" within the microsphere and their subsequent re-illumination of the object [27].

To the best of our knowledge, no prior experimental studies have investigated the effect of polarized light using MAM on anisotropic plasmonic samples such as oriented silver nanowire monolayers. In 2023, Hüser *et al.* conducted a full simulation of microcylinder-assisted interference microscopy, which revealed that for transverse magnetic (TM) polarization, the contrast is higher than for transverse electric (TE) polarization and experimentally validated the modelling [28]. This study corroborates the experimental results of MAM obtained by Darafsheh *et al.* in 2012, who investigated the impact of polarization on the imaging of a blue ray disk using immersed MAM [29]. However, a direct comparison between the two studies is challenging due to the use of different imaging characteristics and polarization effects resulting from the use of microcylinders and microspheres, respectively [26]. Some other studies with MAM have been conducted on holographic gratings to extract the Mueller matrix, but with coherent light [30].

In this context, we have developed a MAM setup for investigating the effect of light polarization on the imaging and reflectance of oriented silver nanowires (AgNWs), selected as the most appropriate anisotropic inorganic 1D nanomaterial for this study due to their common use in a variety of nanoscale devices and applications. This is largely due to their unique chemical and physical properties, most notably their optical properties, reflectance polarization dependence, and localized surface plasmon resonance (LSPR) in the UV–vis spectrum [31–33]. The assembly of these components into anisotropic thin films results in the formation of even more intriguing materials, wherein the optical response is significantly influenced by the orientation and spacing of the metal nanowires. When the AgNWs are aligned, the optical response of these arrays exhibits a pronounced dependence on light polarization, due to the presence of polarization-dependent longitudinal and transverse modes of the localized surface plasmon resonance [32–34]. It is important to note that in this work the microsphere itself, being made of isotropic dielectric material (silica), is not affected by the polarization of the incident light; instead, the observed contrast and imaging variations stem solely from the polarization-dependent optical response of the sample.

2. Materials and methods

Two AgNW sample preparation techniques were employed to produce oriented AgNW monolayers with varying geometries. The first is based on the combination of layer-by-layer assembly [31], which allows control of the deposited material sequence, and grazing incidence spraying (GIS) [25–27], which provides unidirectional alignment of the anisometric nano-objects in each layer. This efficient technique enables the formation of oriented monolayers of anisometric metallic nano-objects, such as AgNWs, aligned in the spray jet direction over areas spanning several square centimeters. Oriented AgNW monolayers were prepared from a suspension of AgNWs in isopropanol (Novarials, 10 mg/mL, diameter: 50 nm, length ~6 μm), diluted 50 times in ultrapure water. The spraying process was conducted using a custom-built spraying system equipped with a 2-fluid nozzle for either 60 or 200 s onto silicon wafers pre-coated with a polymer film ending with a poly (ethylene imine) (PEI) layer (Fig. 1a) [34,35]. The angle between the spray cone's central axis and the substrate was set at 20°, the liquid flow rate at 1 mL/min, and the air flow rate at 30 L/min. Following deposition of the oriented AgNW monolayer, the substrate was rinsed by orthogonal spraying with ultrapure water to remove weakly adsorbed nanoparticles and then dried with compressed air. Fig. 1b shows a Scanning Electron Microscopy (SEM, Hitachi SU8010, operated at 1 keV with the SE-in lens detector) image of an oriented AgNW monolayer obtained with a spray duration of 200 s. While this approach leads to a highly ordered orientation of the AgNWs in the spray direction, it does not yield a perfect uniform distribution of the AgNWs, as shown in the SEM image (Fig. 1b) and its 2D Fourier transform (Fig. 1b, inset), complicating the assessment of the MAM performance.

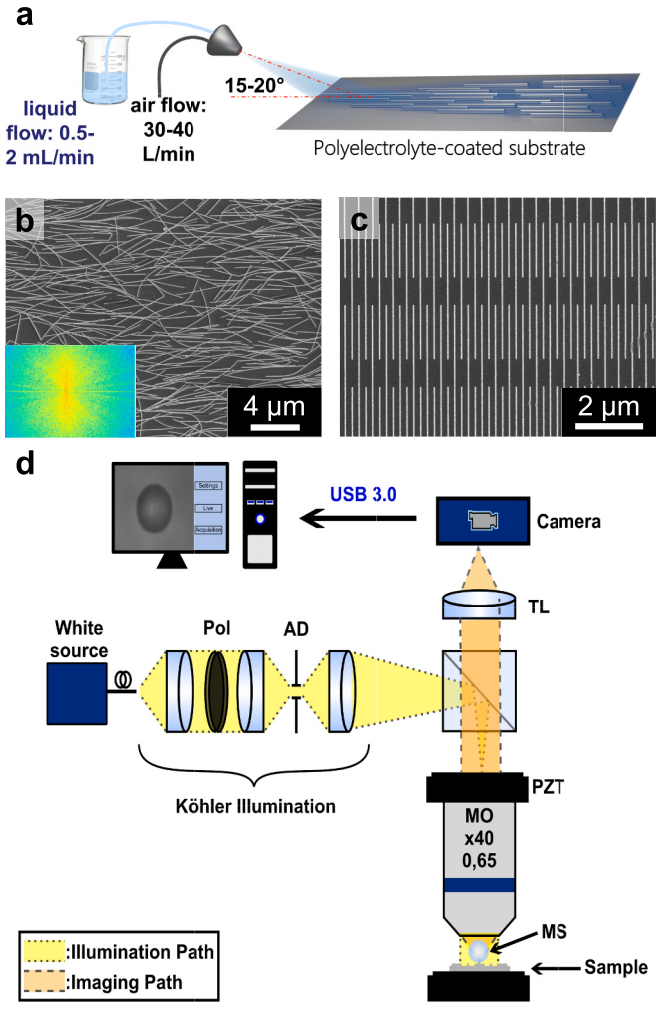

Fig. 1. a) Schematic representation of the GIS setup used for sample preparation, showing a spray nozzle which is fed by the suspension of the AgNWs at a liquid flow rate of 1 mL/min and by compressed air at a flow rate of 30 L/min. Spraying is performed at a low angle onto a polyelectrolyte-coated substrate, which induces AgNW orientation due to shear forces of the flowing liquid [31,32]. b) SEM image of a sample prepared by GIS showing AgNWs aligned in the spray jet direction and inset: 2D Fourier transform of this image reflecting the degree of alignment present in the sample. c) SEM image of an interdigitated grating with a small period of 170 nm (indicated by blue lines) and a larger period of 340 nm (indicated by red lines) prepared by e-beam lithography. d) Schematic representation of the home-built MAM setup (the polarizer (Pol) is not added, unless otherwise stated). (For interpretation of the references to color in this figure legend, the reader is referred to the web version of this article.)

A second preparation technique, e-beam lithography (EBL), was therefore used to produce perfectly aligned AgNW samples for reference. This involves cleaning and drying a 2 × 2 cm^2 silicon wafer, followed by spin-coating a 170 nm thick poly(methyl methacrylate) (PMMA) layer. Electron-beam lithography was then performed using a Raith Voyager system at 50 kV. After developing in a 1:3 mixture of methyl isobutyl ketone and isopropyl alcohol, the substrate was placed in an evaporator for the deposition of 5 nm of chromium (Cr) as an adhesion layer and 45 nm of silver (Ag). The lift-off process was conducted in an n-methyl-2-pyrrolidone ultrasonic bath. The deposited pattern consisted of 100 × 100 μm^2 arrays of interdigitated Ag nanowires, 5 μm long and 50 nm wide, with periodicities ranging from 80 nm to 1 μm. Fig. 1c shows an example of an interdigitated structure observed by SEM with two periods: 170 and 340 nm.

The optical setup used (Fig. 1d) is a home-built vertical column light microscope comprising a white light source with large spectrum (Ocean Optics HL2000) and a Köhler system to provide uniform illumination. Köhler illumination also allows the use of an aperture diaphragm (AD) in the case of MAM [11]. A microscope objective (MO) with a 40 × magnification, with a working distance of 0.36 mm and an NA of 0.65 was employed. The objective is mounted on a piezoelectric stepper (PZT) (PIFOC P-721.C20), which allows positioning within 10 nm. Image acquisition was carried out using a ZWO ASI178 MM camera with a 16-bit CMOS monochrome sensor (3096 × 2080 pixels, with a pixel size of 2.4 μm).

The sample is mounted on a two-axis goniometer to adjust its orientation relative to the illumination. The data acquisition and measurement processing are controlled by Igor Pro software from Wavemetrics. The measured central wavelength of the spectral transfer function of the optical setup is approximately $\lambda_{eff} = 580$ nm, considering the source and the complete optical setup.

To initially ascertain the lateral resolution of the home-made setup before adding the microsphere, a calibrated contrast square grating with a duty cycle of 0.5 (silicon lines on glass) and periods varying between 200 nm and 5 μm, with increments of 200 nm, was utilized. The fabrication and calibration processes of this grating were also validated through light and electron microscopy, revealing a lateral resolution between 600 and 800 nm, depending on the grating periods used.

The microsphere used in our study was a 30 μm silica microsphere, manufactured by Cospheric, which was selected to optimize imaging resolution and performance. As noted by W. Jiang *et al.*, microspheres should be positioned closely together without overlap to maximize the amount of sample information collected [35]. Various techniques have been explored to manipulate microspheres, including mechanical methods such as capillary microprobes [36] or AFM cantilevers [37], optical methods such as fibered microspheres [38], or laser tweezers [39], and chemical approaches such as swimming microrobot optical nanoscopy developed by J. Li *et al.* in 2016 [40]. In our case, the microsphere was initially placed on the sample via a straightforward deposition process, employing an optical fiber for precise positioning. For optimal super-resolution imaging, the microsphere should be in direct contact with the sample or placed at a distance smaller than the wavelength of light. This arrangement ensures effective coupling of evanescent waves, which is critical for achieving the enhanced resolution observed in this study [15].

The objective then is carefully positioned while observing through the microsphere until an image gradually comes into view. The quality of this image depends significantly on the precise position of the objective relative to the microsphere on the sample, the best image appearing at the highest contrast. While moving the objective from its optimum position provides greater magnification, this is at the cost of a significant reduction in contrast. To determine the optimum position, the incident light beam on the microsphere is first focused by opening the aperture diaphragm, thereby ensuring optimal illumination and, consequently, the best lateral resolution. Next, a video is recorded at a high frame rate while moving the objective downwards through the optimal position using the piezoelectric stepper to find the virtual image. ImageJ software is then used to determine the magnification and contrast.

3. Experimental results

3.1. Magnification and contrast

The magnification is determined through a straightforward process by beginning with the calibrated contrast square grating previously mentioned. Using ImageJ, the number of pixels corresponding to a single period of the grating is then measured. Next, a microsphere is introduced into the setup and this measurement is repeated for each position of the objective over a distance of about 15 μm. For greater magnifications, the same grating period spans more pixels. By comparing the number of pixels measured with and without the microsphere, the magnification can be accurately calculated. The contrast is calculated by extracting cross-sections from the virtual image using the formula $\frac{C_{Max}-C_{Min}}{C_{Max}+C_{Min}}$, where C_{Max} and C_{Min} are the maximum and minimum pixel values respectively. A statistical study was conducted to obtain the standard deviation of the dataset. Finally, using calculations for the pixel size and with a known period of the grating studied, the graph shown in Fig. 2a was obtained, indicating that the highest contrast is achieved at a position for which the magnification is × 7.

Once the magnification resulting from the microspheres is known, the lateral resolution enhancement can be determined through the use of the contrast transfer function (CTF) [2]. By employing this methodology with the previously mentioned calibrated contrast grating and a 30 μm glass microsphere (Fig. 2b), the resolution of the setup with a microsphere is approximately 340 nm (grating period resolved). This represents an enhancement of between 2 and 2.7 times compared to the lateral resolution measured without the microsphere.

MAM under non-polarized light was first used to image oriented AgNW monolayers prepared by e-beam lithography. The SEM image in Fig. 1c shows the two interdigitated sets of nanowires, one with the larger period of 340 nm (indicated by red lines) and the other with the smaller period of 170 nm (blue lines). While direct observation using the objective alone revealed vertical stripes corresponding to the positions of the two sets of gratings, no details of individual horizontal nanowires could be resolved (Fig. 2c). The introduction of a 30 μm microsphere into the optical path alone did not significantly enhance the resolution.

3.2. Polarization dependent MAM resolution

The sample was then observed through the microsphere with linearly polarized light by adding a polarizer into the illumination arm. Rotating the polarizer allowed selectively exciting the longitudinal and transverse modes of the localized plasmonic resonances of the AgNWs [33,34]. Transverse electric (TE- or s-) polarized light, with the electric field aligned parallel to the nanowire axis, excites the longitudinal LSPR mode. Conversely, transverse magnetic (TM- or p-) polarized light, with the electric field perpendicular to the nanowire axis, excites the transverse LSPR mode (Fig. 3a).

The reflectance of the silver nanowire grating was simulated using Reticolo, an open-access freeware that employs rigorous coupled wave analysis (RCWA) for both 1D (classical and conical diffraction) and 2D crossed gratings (Fig. 3b) [41]. The AgNW monolayers were studied in two dimensions, using tabulated data for the refractive index of bulk silver, chromium and silicon [42].

The reflectance of the GIS sample was measured using a commercial UV–vis spectrometer (Cary 5000, Agilent) with a 5 mm beam diameter (Fig. 3c). Both the GIS and e-beam lithography samples exhibit polarization-dependent reflectance, with clear distinctions between TE and TM polarizations. Although the absolute reflectance values differ due to the differences in sample geometry and fabrication method, the

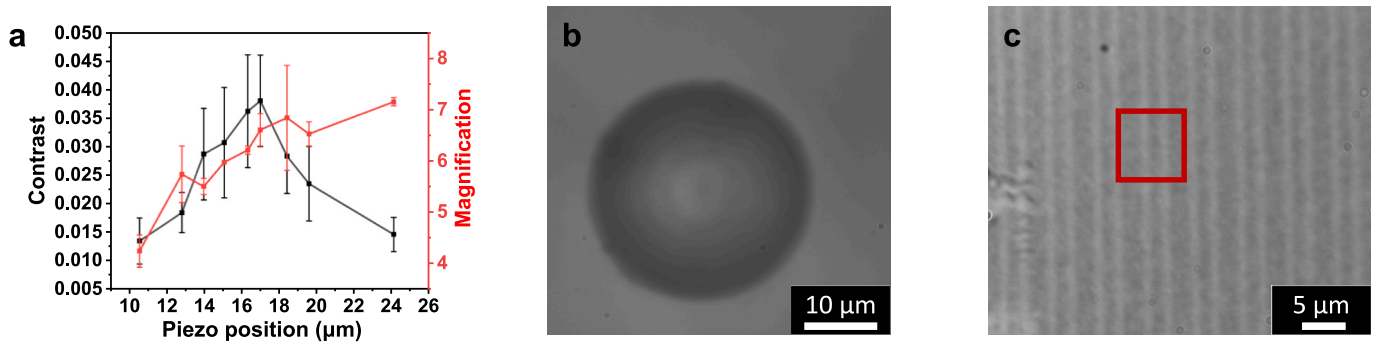

Fig. 2. a)Magnification and contrast obtained with a calibrated contrast square grating as a function of the piezo position to determine the optimal position of the microsphere for imaging. b) Optical image of a microsphere with a size of ~ 30 µm. c) Optical image of the interdigitated sample (see Fig. 1c) imaged without the microsphere and with non-polarized light, unable to resolve either grating period. The red square shows the zone observed with the microsphere. (For interpretation of the references to color in this figure legend, the reader is referred to the web version of this article.)

experimental reflectance spectra of the oriented AgNW array obtained by GIS (Fig. 3c) show good qualitative agreement with the spectra simlulated for a geometry identical to the oriented AgNW array obtained by EBL (Fig. 3b), particularly in terms of polarization-dependent trends and the presence of transverse plasmon resonances. Under TM-polarized illumination, the transverse localized surface plasmon resonance (LSPR) mode is excited in the near-UV region [33,34,43], resulting in a reduction in reflectance due to increased absorption by the silver nanowires (AgNWs). This resonance occurs at 362 nm for the e-beam lithography sample, where reflectance reaches a minimum of 16 %, while the GIS sample exhibits a resonance at 350 nm with a minimum reflectance of 38 %. In contrast, TE-polarized illumination excites the longitudinal LSPR mode in the visible to near-infrared region [33,34,43], which interestingly leads to an increased reflectance. This enhancement is attributed to the negative real part of the effective dielectric function of the oriented AgNW monolayer [33,44], imparting metallic-like reflective properties. Overall, the reflectance under TE polarization exceeds that under TM polarization across both the UV and visible spectral regions. As a result, samples are expected to appear clearer and brighter under TE-polarized light during optical imaging.

This polarization-dependent contrast was confirmed by microsphere-assisted imaging (Fig. 3d and e), as the image clarity significantly improved when light was polarized parallel to the AgNW axis (TE-polarized). For the sample prepared by e-beam lithography, this configuration allowed for clear resolution of individual nanowires within the larger-period grating (340 nm), while the smaller-period grating (170 nm) remained unresolved (Fig. 3d and inset). The high reflectance of AgNWs under TE polarization enabled their clear visualization in both sample types. However, under TM polarization, nanowires were no longer discernible in the e-beam lithography sample (Fig. 3d) since the reflectance of the AgNWs is almost the same as that of the silicon substrate in the visible range, as displayed on the reflectance spectrum (Fig. 3b). In the case of the samples obtained by GIS, some clearer structures can be observed, but these are much less visible than in the TE mode. Given that the GIS technique does not perfectly align the nanowires and that there is some degree of aggregation (Fig. 1b), the brighter structures observed are more likely to be aggregates rather than single nanowires, especially given the resolution measured for the MAM system.

This interpretation is also supported by recent studies, such as that of Hamans *et al.* (2022), who demonstrated that the optical response of individual silver nanowires is highly sensitive to light polarization [45]. Their study revealed distinct UV plasmonic peaks under perpendicular polarization, corresponding to transverse plasmon modes. The extinction is dominated by scattering. These modes induce changes in the local electric field distribution, directly contributing to the contrast variation observed in polarized imaging of aligned nanowires. In addition to high reflectance, other factors contribute to the observation of the samples. These include the near-field enhancement induced by the microsphere as previously explained in the literature [10–13], which improves the spatial resolution and contrast of the imaging, as well as the uniform alignment of the nanowires, which amplifies the polarization effect.

Although plasmonic resonance plays a key role in the observed polarization-dependent contrast in AgNWs, similar effects might be observed in non-plasmonic materials, such as semiconductors, due to polarization-dependent light scattering [46–48]. This suggests that polarization, combined with microspheres, could be an effective tool for enhancing contrast even in the absence of plasmonic behavior.

In conclusion, the resolution performance of a home-built MAM system has been investigated using a standard objective (×40, NA = 0.65) and 30 µm diameter silica microsphere under polarized light. The study of two types of samples of AgNWs, one made by a bottom-up approach and the other by e-beam lithography, showed that the lateral resolution of the system was enhanced by a factor between 2 and 2.7, enabling the successful imaging of a grating of 340 nm, which could not be resolved without the microsphere. Although MAM does not reach the resolution levels of some advanced super-resolution techniques that can resolve up to 20 nm in the case of STED for example [49], it provides a compelling trade-off by avoiding fluorescent labeling and complex preparation protocols.. Compared to Structured Illumination Microscopy (SIM), MAM is also significantly faster and simpler, as SIM requires multiple image acquisitions and computational reconstruction involving specialized software [44,50]. The use of polarized light with microspheres shows significant potential for characterizing anisotropic nanoscale structures. Further resolution enhancement could be achieved by reducing the microsphere size and using an immersion objective to provide more details of nanoscale features using optical microscopy without labelling.

Data availability: The data that supports the findings of this study are available from the corresponding author upon reasonable request.

CRediT authorship contribution statement

Farid Mahfoud: Writing – review & editing, Writing – original draft, Visualization, Validation, Resources, Methodology, Investigation, Formal analysis, Data curation, Conceptualization. **Christophe Cordier:** Validation, Methodology, Investigation, Formal analysis, Data curation, Conceptualization. **Sebastien Marbach:** Validation, Supervision, Project administration, Methodology, Formal analysis, Conceptualization. **Michel Tschopp:** Validation, Methodology, Formal analysis. **Paul Montgomery:** Writing – review & editing, Project administration, Funding acquisition, Conceptualization. **Olivier Felix:** Writing – review & editing, Validation, Supervision, Resources, Project administration, Funding acquisition, Formal analysis, Conceptualization. **Matthias Pauly:** Writing – review & editing, Supervision, Resources, Project administration, Funding acquisition, Formal analysis,

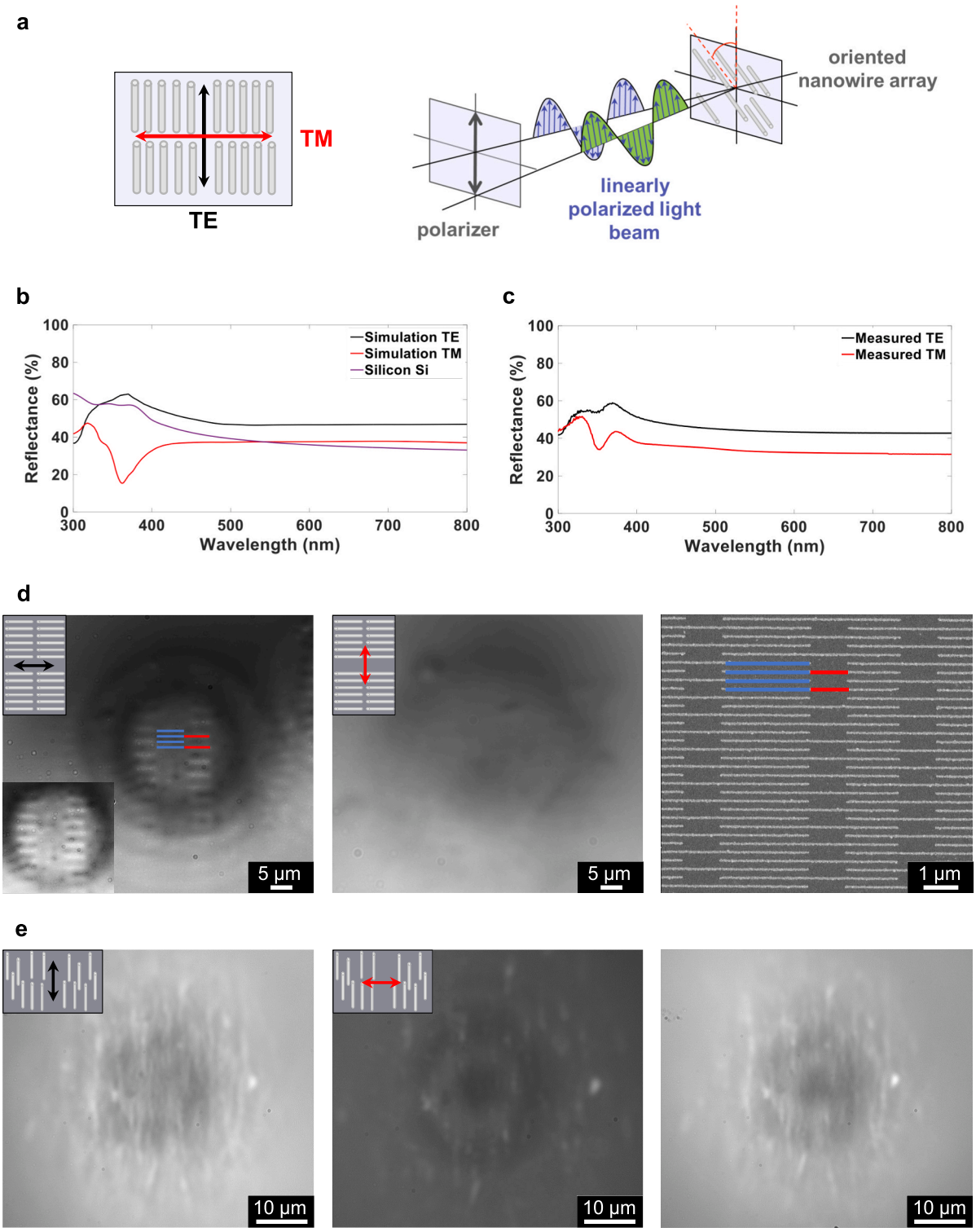

Fig. 3. a) Sketch showing the direction of the electric field with respect to the nanowire orientation for TE and TM polarized light. b) Simulated polarized reflectance spectrum of an agnw grating with dimensions corresponding to the sample prepared by e-beam lithography showing the reflectance for TE and TM-polarized light and comparing it with the reflectance of silicon. c) Measured polarized reflectance spectrum of an AgNW monolayer prepared by GIS showing the reflectance for TE- and TM-polarized light. d) SEM image (right) of an interdigitated grating prepared by e-beam lithography with a color code showing the period of 340 nm and the corresponding optical images observed through a microsphere with TE (left) Inset: contrast enhanced image from the center of the microsphere, and TM polarizations (middle). e) Optical images of the oriented AgNW monolayer prepared by GIS observed through a microsphere without polarization (right), and with TE (left) and TM (middle) polarizations.

Conceptualization. **Manuel Flury:** Writing – review & editing, Validation, Supervision, Resources, Project administration, Methodology, Investigation, Funding acquisition, Formal analysis, Data curation, Conceptualization.

Declaration of competing interest

The authors declare that they have no known competing financial interests or personal relationships that could have appeared to influence the work reported in this paper.

Acknowledgments

This work of the Interdisciplinary Institute HiFunMat, as part of the ITI 2021-2028 program of the University of Strasbourg, CNRS and Inserm, was supported by IdEx Unistra (ANR-10-IDEX-0002) and SFRI (STRAT'US project, ANR-20-SFRI-0012) under the framework of the French Investments for the Future Program. We acknowledge the KNMF (Karlsruhe Nano Micro Facility) for sample fabrication, the electron microscopy core facility PLAMICS and the analysis core facility CarMac of the Institut Charles Sadron. The authors are also grateful to Prof. Sylvain Lecler for fruitful discussions and providing insights on this subject.

Appendix A. Supplementary data

Supplementary data to this article can be found online at https://doi.org/10.1016/j.optlastec.2025.113383.

Data availability

Data will be made available on request.

References

[1] J. Vangindertael, R. Camacho, W. Sempels, H. Mizuno, P. Dedecker, K.P.F. Janssen, An introduction to optical super-resolution microscopy for the adventurous biologist, Methods Appl Fluoresc 6 (2018) 022003, https://doi.org/10.1088/2050-6120/aaae0c.
[2] S. Marbach, P. Montgomery, M. Flury, Microsphere-assisted multispectral microscopy, Opt. Lasers Eng. 180 (2024) 108299, https://doi.org/10.1016/j.optlaseng.2024.108299.
[3] X. Hao, C. Kuang, Z. Gu, Y. Wang, S. Li, Y. Ku, et al., From microscopy to nanoscopy via visible light, Light Sci. Appl. 2 (2013) e108–e, https://doi.org/10.1038/lsa.2013.64.
[4] P.C. Montgomery, S. Lecler, A. Leong-Hoï, S. Perrin, High Resolution Surface Metrology using Microsphere-Assisted Interference Microscopy, Phys. Status Solidi A 216 (2019) 1800761, https://doi.org/10.1002/pssa.201800761.
[5] S.T. Hess, T.P.K. Girirajan, M.D. Mason, Ultra-High Resolution Imaging by Fluorescence Photoactivation Localization Microscopy, Biophys. J . 91 (2006) 4258–4272, https://doi.org/10.1529/biophysj.106.091116.
[6] M.J. Rust, M. Bates, X. Zhuang, Sub-diffraction-limit imaging by stochastic optical reconstruction microscopy (STORM), Nat. Methods 3 (2006) 793–796, https://doi.org/10.1038/nmeth929.
[7] S.W. Hell, J. Wichmann, Breaking the diffraction resolution limit by stimulated emission: stimulated-emission-depletion fluorescence microscopy, Opt. Lett. 19 (1994) 780–782, https://doi.org/10.1364/OL.19.000780.
[8] C. Jiang, H. Yue, B. Yan, T. Dong, X. Cui, P. Chen, et al., Label-free non-invasive subwavelength-resolution imaging using yeast cells as biological lenses, Biomed. Opt. Express 12 (2021) 7113–7121, https://doi.org/10.1364/BOE.437965.
[9] Wang Z, Guo W, Li L, Luk'yanchuk B, Khan A, Liu Z, et al. Optical virtual imaging at 50 nm lateral resolution with a white-light nanoscope. Nat Commun 2011;2:218. doi: 10.1038/ncomms1211.
[10] S. Lecler, S. Perrin, A. Leong-Hoi, P. Montgomery, Photonic Jet Lens. Sci Rep 9 (2019) 4725, https://doi.org/10.1038/s41598-019-41193-2.
[11] V.N. Astratov, Y.B. Sahel, Y.C. Eldar, L. Huang, A. Ozcan, N. Zheludev, et al., Roadmap on Label-Free Super-Resolution Imaging, Laser Photonics Rev. 17 (2023) 2200029, https://doi.org/10.1002/lpor.202200029.
[12] H. Yang, R. Trouillon, G. Huszka, M.A.M. Gijs, Super-Resolution Imaging of a Dielectric Microsphere is Governed by the Waist of its Photonic Nanojet, Nano Lett. 16 (2016) 4862–4870, https://doi.org/10.1021/acs.nanolett.6b01255.
[13] A.V. Maslov, V.N. Astratov, Resolution and Reciprocity in Microspherical Nanoscopy: Point-Spread Function Versus Photonic Nanojets, Phys. Rev. Appl 11 (2019) 064004, https://doi.org/10.1103/PhysRevApplied.11.064004.
[14] R. Boudoukha, S. Perrin, A. Demagh, P. Montgomery, N.-E. Demagh, S. Lecler, Near- to Far-Field Coupling of Evanescent Waves by Glass Microspheres, Photonics 8 (2021) 73, https://doi.org/10.3390/photonics8030073.
[15] R. Boudoukha, S. Perrin, A. Guessoum, N.-E. Demagh, P. Montgomery, S. Lecler, Evanescent point sources: application to microsphere-assisted super-resolution microscopy, Opt. Lett. 49 (2024) 6429, https://doi.org/10.1364/OL.542794.
[16] S. Perrin, H. Li, A. Leong-Hoi, S. Lecler, P. Montgomery, Illumination conditions in microsphere-assisted microscopy, J. Microsc. 274 (2019) 69–75, https://doi.org/10.1111/jmi.12781.
[17] S. Perrin, H. Li, K. Badu, T. Comparon, G. Quaranta, N. Messaddeq, et al., Transmission Microsphere-Assisted Dark-Field Microscopy, Phys Status Solidi RRL – Rapid Res Lett 13 (2019) 1800445, https://doi.org/10.1002/pssr.201800445.
[18] Q. Lin, D. Wang, Y. Wang, L. Rong, J. Zhao, S. Guo, et al., Super-resolution imaging by microsphere-assisted optical microscopy, Opt. Quantum Electron. 48 (2016) 557, https://doi.org/10.1007/s11082-016-0833-2.
[19] F. Wang, L. Liu, P. Yu, Z. Liu, H. Yu, Y. Wang, et al., Three-Dimensional Super-Resolution Morphology by Near-Field Assisted White-Light Interferometry, Sci. Rep. 6 (2016) 24703, https://doi.org/10.1038/srep24703.
[20] G. Wu, M. Hong, Optical Microsphere Nano-Imaging: Progress and challenges, Engineering 36 (2024) 102–123, https://doi.org/10.1016/j.eng.2023.10.019.
[21] N. Upreti, G. Jin, J. Rich, R. Zhong, J. Mai, C. Zhao, et al., Advances in Microsphere-based Super-Resolution Imaging, IEEE Rev. Biomed. Eng. 18 (2025) 337–349, https://doi.org/10.1109/RBME.2024.3355875.
[22] Marchand R, Ortkrass H, Aziz D, Pfanner F, Abbas E, Hübner W, et al. Super-resoluon Live-cell Fluorescence Lifeme Imaging n.d.
[23] V. Abbasian, V. Farzam Rad, A. Darafsheh, Microsphere-assisted laser speckle polarimetric microscopy, J. Appl. Phys. 137 (2025) 063104, https://doi.org/10.1063/5.0244195.
[24] J. Park, Y. Choi, S. Kwon, Y. Lee, J. Kim, J. Kim, et al., Microsphere-assisted hyperspectral imaging: super-resolution, non-destructive metrology for semiconductor devices, Light Sci. Appl. 13 (2024) 122, https://doi.org/10.1038/s41377-024-01469-3.
[25] L. Hüser, T. Pahl, S. Hagemeier, T. Eckhardt, F. Rosenthal, M. Diehl, et al., Microsphere-assistance in conventional, interference and confocal microscopy – modeling and experimental results, J Eur Opt Soc-Rapid Publ 21 (2025) 16, https://doi.org/10.1051/jeos/2025011.
[26] V. Abbasian, T. Pahl, L. Hüser, S. Lecler, P. Montgomery, P. Lehmann, et al., Microsphere-assisted quantitative phase microscopy: a review, Light Adv Manuf 5 (2024) 1, https://doi.org/10.37188/lam.2024.006.
[27] A.V. Maslov, V.N. Astratov, Origin of the super-resolution of microsphere-assisted imaging, Appl. Phys. Lett. 124 (2024) 061105, https://doi.org/10.1063/5.0188450.
[28] L. Hüser, T. Pahl, P. Lehmann, Experimental and numerical polarization analysis of the 3D transfer behavior in microsphere-assisted interferometry for 1D phase gratings, J Eur Opt Soc-Rapid Publ 19 (2023) 32, https://doi.org/10.1051/jeos/2023029.
[29] A. Darafsheh, G.F. Walsh, L. Dal Negro, V.N. Astratov, Optical super-resolution by high-index liquid-immersed microspheres, Appl. Phys. Lett. 101 (2012) 141128, https://doi.org/10.1063/1.4757600.
[30] V. Abbasian, A.-R. Moradi, Microsphere-assisted super-resolved Mueller matrix microscopy, Opt. Lett. 45 (2020) 4336, https://doi.org/10.1364/OL.395735.
[31] G. Decher, Fuzzy Nanoassemblies: Toward Layered Polymeric Multicomposites, Science 277 (1997) 1232–1237.
[32] H. Hu, M. Pauly, O. Felix, G. Decher, Spray-assisted alignment of Layer-by-Layer assembled silver nanowires: a general approach for the preparation of highly anisotropic nano-composite films, Nanoscale 9 (2017) 1307–1314, https://doi.org/10.1039/C6NR08045F.
[33] W. Wu, Y. Battie, V. Lemaire, G. Decher, M. Pauly, Structure-Dependent Chiroptical Properties of Twisted Multilayered Silver Nanowire Assemblies, Nano Lett. 21 (2021) 8298–8303, https://doi.org/10.1021/acs.nanolett.1c02812.
[34] H. Hu, S. Sekar, W. Wu, Y. Battie, V. Lemaire, O. Arteaga, et al., Nanoscale Bouligand Multilayers: Giant Circular Dichroism of Helical Assemblies of Plasmonic 1D Nano-Objects, ACS Nano 15 (2021) 13653–13661, https://doi.org/10.1021/acsnano.1c04804.
[35] W. Jiang, J. Wang, Y. Yang, Y. Bu, A Review of Microsphere Super-Resolution Imaging Techniques, Sensors 24 (2024) 2511, https://doi.org/10.3390/s24082511.
[36] L.A. Krivitsky, J.J. Wang, Z. Wang, B. Luk'yanchuk, Locomotion of microspheres for super-resolution imaging, Sci. Rep. 3 (2013) 3501, https://doi.org/10.1038/srep03501.
[37] S. Wang, D. Zhang, H. Zhang, X. Han, R. Xu, Super-resolution optical microscopy based on scannable cantilever-combined microsphere, Microsc. Res. Tech. 78 (2015) 1128–1132, https://doi.org/10.1002/jemt.22595.
[38] T. Hajj, S. Marbach, P. Pfeiffer, P. Montgomery, S. Lecler, M. Flury, High-quality manipulable fiber-microsphere for super-resolution microscopy, Opt. Lett. 48 (2023) 2222–2225, https://doi.org/10.1364/OL.484399.
[39] Y. Wen, H. Yu, W. Zhao, P. Li, F. Wang, Z. Ge, et al., Scanning Super-Resolution Imaging in Enclosed Environment by Laser Tweezer Controlled Superlens, Biophys. J . 119 (2020) 2451–2460, https://doi.org/10.1016/j.bpj.2020.10.032.
[40] J. Li, W. Liu, T. Li, I. Rozen, J. Zhao, B. Bahari, et al., Swimming Microrobot Optical Nanoscopy, Nano Lett. 16 (2016) 6604–6609, https://doi.org/10.1021/acs.nanolett.6b03303.
[41] P. Lalane, J.-P. Hugonin, Light-in-complex-nanostructures/RETICOLO: V9, Zenodo (2021), https://doi.org/10.5281/zenodo.4419063.
[42] M.N. Polyanskiy, Refractiveindex.info database of optical constants, Sci. Data 11 (2024) 94, https://doi.org/10.1038/s41597-023-02898-2.

[43] W. Wu, M. Pauly, Chiral plasmonic nanostructures: recent advances in their synthesis and applications, Mater. Adv. 3 (2022) 186–215, https://doi.org/10.1039/D1MA00915J.
[44] J. Kanungo, J. Schilling, Experimental determination of the principal dielectric functions in silver nanowire metamaterials, Appl. Phys. Lett. 97 (2010) 021903, https://doi.org/10.1063/1.3462311.
[45] R.F. Hamans, M. Parente, A. Garcia-Etxarri, A. Baldi, Optical Properties of Colloidal Silver Nanowires, J. Phys. Chem. C 126 (2022) 8703–8709, https://doi.org/10.1021/acs.jpcc.2c01251.
[46] M.M. Adachi, M.P. Anantram, K.S. Karim, Optical Properties of Crystalline−Amorphous Core−Shell Silicon Nanowires, Nano Lett. 10 (2010) 4093–4098, https://doi.org/10.1021/nl102183x.
[47] G. Brönstrup, N. Jahr, C. Leiterer, A. Csáki, W. Fritzsche, S. Christiansen, Optical Properties of Individual Silicon Nanowires for Photonic Devices, ACS Nano 4 (2010) 7113–7122, https://doi.org/10.1021/nn101076t.
[48] H.-C. Lee, S.-J. Lee, J. Kim, K.-H. Kim, J.-S. Park, M.-S. Hwang, et al., Unique Scattering Properties of Silicon Nanowires embedded with Porous Segments, ACS Appl. Mater. Interfaces 11 (2019) 21094–21099, https://doi.org/10.1021/acsami.9b04680.
[49] Trifonov AS, Jaskula J-C, Teulon C, Glenn DR, Bar-Gill N, Walsworth RL. Limits to Resolution of CW STED Microscopy. Adv. At. Mol. Opt. Phys., vol. 62, Elsevier; 2013, p. 279–302. doi: 10.1016/B978-0-12-408090-4.00005-0.
[50] R. Lin, E.T. Kipreos, J. Zhu, C.H. Khang, P. Kner, Subcellular three-dimensional imaging deep through multicellular thick samples by structured illumination microscopy and adaptive optics, Nat. Commun. 12 (2021) 3148, https://doi.org/10.1038/s41467-021-23449-6.